Progress In Electromagnetics Research, Vol. 116, 313–331, 2011

TIME-DOMAIN MEASUREMENT OF TIME-CODED UWB CHIPLESS RFID TAGS

A. Ramos, A. Lazaro, D. Girbau, and R. Villarino

Department of Electronics, Electrics and Automatics Engineering
Universitat Rovira i Virgili (URV)
Av. Països Catalans 26, Campus Sescelades, Tarragona 43007, Spain

Abstract—Chipless ultra-wideband (UWB) has been proposed as a low-cost alternative for radiofrequency identification (RFID). In this paper, a comprehensible theoretical introduction to time-domain operation of a UWB RFID tag is described, and a circuit model is proposed. For commercial applications low-cost RFID readers are demanded. To this end, this paper addresses the measurement of time-coded UWB chipless tags for RFID in time domain. Two different setups to detect time-coded tags are presented, one based on commercial UWB impulse radar (IR) and the other based on a vector network analyzer (VNA). The experimental results show the feasibility of using an IR-UWB radar as a UWB RFID reader, achieving very good read ranges.

1. INTRODUCTION

A RFID system consists of readers and tags applied to objects. The reader interrogates the tags via a wireless link to obtain the data stored into them [1]. The cheapest RFID tags with the largest commercial potential are passive or semipassive [2, 3], where the energy necessary for tag–reader communication is harvested from the reader's signal. Passive RFID tags are based on backscatter modulation, where the antenna reflection properties are changed according to information data.

UHF passive tags are preferred due to the compromise between price, memory capacity and read range in front of HF and MF frequency tags, which are reserved for short-range applications.

Received 30 March 2011, Accepted 1 May 2011, Scheduled 6 May 2011
Corresponding author: Antonio Lazaro (antonioramon.lazaro@urv.cat).

However, UHF RFID technology has some drawbacks. The frequency band allocation and transmission power permitted depend on the country or region, and the technology has reduced area coverage, an insufficient range resolution for accurate localization and a scarce multiple-access capability. In addition, UHF RFID technology is also influenced by multipath propagation [4], interference between readers [5] and frequency detuning when tags are attached to materials [6].

Since the FCC's allocation of UWB spectrum in the range 3.1–10.6 GHz in 2002, UWB has gained interest in academia [7] and industry [8]. UWB has several advantages when compared to traditional narrow-band communication systems such as high data-rate, low average radiated power and simple RF circuitry. Many of these potential advantages are a direct consequence of UWB's large instantaneous bandwidth. UWB technology is also a promising solution for next generation RFID systems to overcome most limitations of current narrow-band RFID technology. A great interest has arisen in UWB active tags for their localization capability in indoor scenarios [9]. However, they are expensive for other applications where short-range requirements (few meters) and low cost are required.

A significant lower in passive UHF tag costs has been achieved within a short period of time due to the adoption of RFID technology in several fields such as logistic, automotive, surveillance, automation systems, etc. [3]. Even so, tag price is limited by the chip and the process to attach it to the antenna. For instance, the use of current chip-based tags is prohibitive for tagging documents and large volumes of paper/plastic-based items such as banknotes, postage stamps, tickets and envelopes.

UWB chipless RFID systems might be a promising solution for low-cost item tagging [10–17]. Chipless tags based on surface acoustic waves (SAW) are already commercially available [18–20]. However, these tags are expensive; they do not provide a fully printable solution due to their piezoelectric nature and can not be applied on banknotes, postage stamps, or other paper/plastic-based items [10]. UWB chipless RFID tags have been recently proposed in [10–16]. In [10, 11], printable chipless RFID tags based on multiresonators have been reported; here information is coded in frequency. An alternative method where the information is coded in time has been proposed in [14–17]. Here, the simplest way to code information is by varying the physical length of an open-ended transmission line connected to a scattering UWB antenna. Although this idea has been proposed by some authors [14–17], there are few experimental results [14–17], which have been obtained by means of high-cost instruments such as vector network analyzers

(VNA). Future implementations of commercial readers should be based on low-cost equipments, such as IR-UWB radars.

The aim of this work is to study the possibility of using an IR-UWB radar as a RFID reader for time-domain chipless UWB RFID. To this end, an experimental setup for time-domain chipless UWB RFID based on a commercial UWB radar is presented. Using UWB antennas connected to a delay line as a tag, several experimental results are obtained that show the basic theory of operation and the potential of this new RFID technology. Experimental results are compared to the ones obtained with a VNA. In contrast with previous measurements reported for scattering antennas [14–17], measurements are here performed in real environments (not inside an anechoic chamber). Read-ranges up to 1.5 meters are demonstrated, which are much larger than the read-ranges in the order of tens of centimeters demonstrated for frequency-coded chipless tags [10, 11].

The paper is organized as follows. Section 2 presents the basic theory of time-coded UWB RFID using a comprehensible circuit interpretation for chipless time-coded tags. Section 3 describes the two time-domain experimental setups proposed, one based on an IR UWB radar and another based on a VNA. In Section 4 results are presented using the experimental setups introduced in Section 3, comparing both responses for identical measurements. Finally, Section 5 gives some conclusions.

2. UWB CHIPLESS RFID OPERATION PRINCIPLE AND SYSTEM THEORY

Passive RFID is based on modulating the radar cross section [21] of the tag. Depending on the authors (Green [22], Collin [23], Hansen [24]), there are different formulations for deriving the field scattered at an antenna connected to an arbitrary load when it is illuminated by a plane wave. However, these authors have shown that this field can be expressed as the sum of two terms (or modes):

- A structural mode, which is mainly due to the wave diffraction at the antenna structure (patches, ground plane, edge effects...) [25–28].
- An antenna mode (or tag mode), which is mainly due to the radiation properties of the antenna. This term depends on the load Z_L connected to the antenna.

In consequence, the field scattered at an antenna $E^S(Z_L)$ connected to an arbitrary load Z_L can be obtained from [29, 30]:

$$\overline{E^S}(Z_L) = \overline{E^{sm}}(Z_c) + \overline{E^{am}}(Z_L) = \overline{E^{sm}}(Z_c) + \frac{\Gamma_L}{1 - \Gamma_L \Gamma_a}\overline{E_0} \quad (1)$$

where $E^{sm}(Z_c)$ is the structural-mode scattering field and $E^{am}(Z_L) = E_0\Gamma_L/(1-\Gamma_L\Gamma_a)$ is the antenna-mode scattering field. Z_c is the normalization impedance, E_0 is the scattering field under an unit incident wave and Γ_a, Γ_L are the reflection coefficients of the antenna and the load, respectively. The reflection coefficient Γ_L, which multiplies the unit-incident-wave scattering field E_0, depends on the circuit connected to the antenna. This circuit not only accounts for the load itself (Z_{LOAD}), but also for the transmission line that connects the antenna and the load. Therefore, the antenna-mode scattering field depends on the load and the length L of this transmission line. When the circuit connected to the antenna is matched ($\Gamma_L = 0$) only structural scattering exists. If not, part of the received energy is reradiated, and structural and antenna modes coexist.

The proposed system is shown in Figure 1. It consists of a bistatic UWB radar that illuminates the tag. When the transmitted pulse hits the tag antenna, a portion is backscattered towards the receiver and a portion propagates inside the tag. Then, time-coded chipless tags can be considered scattering antennas (antennas terminated with a load impedance) with two scattering modes: the structural mode (first or early-time reflection) and the tag (or antenna) mode (second reflection).

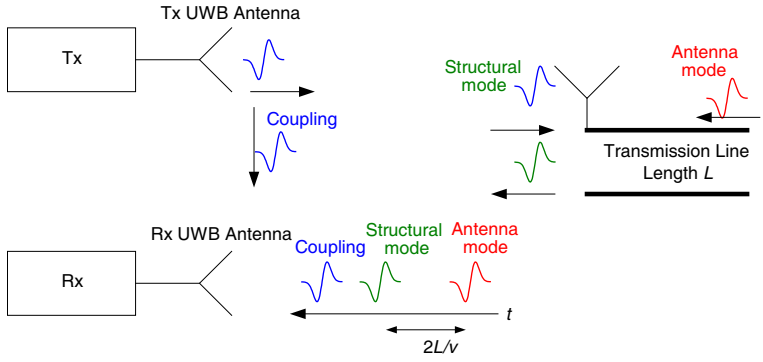

Figure 1. Experimental RFID system based on a UWB radar for time-coded chipless tags measurement.

An in-depth comprehensive circuit-theory for UWB time-coded chipless tags is given next. The tag is modeled as an equivalent two-port network (antenna) terminated with a transmission line of length L and characteristic impedance Z_c loaded with an impedance Z_{LOAD} [23], as presented in Figure 2. The wave a represents the incoming wave from the radar transmitting antenna. The outcoming

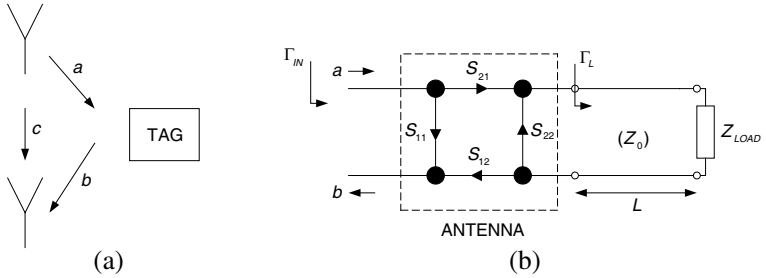

Figure 2. Model for the UWB RFID tag.

wave b is generated due to reflection and is scattered in direction to the radar receiving antenna. The waves a and b are normalized to the free-space impedance ($120\pi\,\Omega$). The output of the antenna is normalized to Z_c. Thus, S_{22} in Figure 2(b) represents the reflection coefficient of the antenna, $S_{22} = \Gamma_a$. The reflection coefficients Γ_a and Γ_L are defined as:

$$\Gamma_a = \frac{Z_a - Z_c}{Z_a + Z_c} \tag{2}$$

$$\Gamma_L = \frac{Z_L - Z_c}{Z_L + Z_c} \tag{3}$$

where Z_a is the antenna impedance and Z_L the load connected to the antenna. The reflection coefficient at the input of the tag Γ_{in} can be obtained from the analysis of Figure 2:

$$\Gamma_{in} = \frac{b}{a} = S_{11} + \frac{\Gamma_L}{1 - \Gamma_a \Gamma_L} S_{21} S_{12} \tag{4}$$

which can be expanded in series:

$$\Gamma_{in} = S_{11} + S_{21} S_{12} \Gamma_L \left[1 + \sum_{n=1}^{\infty} (\Gamma_a \Gamma_L)^n \right] \approx S_{11} + S_{21} S_{12} \Gamma_L \tag{5}$$

Assuming that the RFID reader transmits a pulse $p(t)$ and defining $\tau_L = 2L/v$ as the round-trip propagation delay along the transmission line (v is the propagation velocity in the transmission line), a physical interpretation of (5) can be obtained from the bounce diagram shown in Figure 3. It is a two-dimensional representation of the transient waves bouncing back and forth on the tag. Zigzagging lines indicate the progress of the wave as a function of position and time (t). The direction of travel is from bottom to top. The terms within the series in (5) represent the multiple reflections of the waves between the load

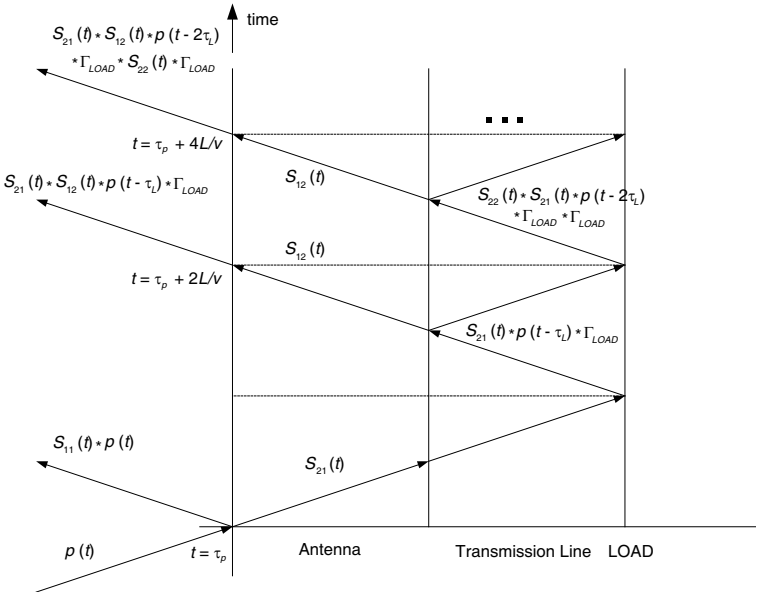

Figure 3. Bounce diagram for transient waves scattered at the tag.

Z_{LOAD} and the antenna, which appear every time delay $n\tau_L$ (for $n = 1, 2, 3 \ldots$). For a well-matched antenna only the first term is considered because the others vanish rapidly. Since delay information in this term is the key parameter, the best method to obtain maximum amplitude is to make $Z_{LOAD} = \infty$ or $Z_{LOAD} = 0$ (open-circuit or short-circuit load) and design Z_c matched to the antenna input impedance Z_a. Assuming a low-loss line:

$$\Gamma_L = e^{-j2\pi f 2L/v} \Gamma_{LOAD} \tag{6}$$

where f is the frequency and Γ_{LOAD} is the reflection coefficient of the load connected at the end of the transmission line, (e.g., $\Gamma_{LOAD} = 1$ when $Z_{LOAD} = \infty$). It can also be seen that the phase of Γ_L, $e^{-j2\pi f 2L/v}$, directly depends on the frequency and increases with the length L. This shows that the load reflection coefficient phase, and therefore the scattered tag (antenna) mode field $E^{am}(Z_L)$ depends on the length of the transmission line before the load.

Moreover, the antenna layout must be carefully designed in order to prevent undesired radiation effects that could influence the antenna-mode field. For instance, in [31, 32] it is reported that the ground size and shape can affect some UWB antennas such as fat monopoles.

By applying Inverse Fourier Transform to (5), we can obtain the time-domain backscattered field or, equivalently, the time-domain

reflection coefficient between the incoming and outcoming waves:

$$\Gamma_{in}(t) \approx S_{11}(t) + S_{12}(t) * S_{21}(t) * \delta(t - \tau_L) * \Im^{-1}(\Gamma_{LOAD}) \quad (7)$$

where $*$ denotes the convolution operator. When Γ_{LOAD} is real, (i.e., resistive or open/short-circuited loads), (7) can be expressed as:

$$\Gamma_{in}(t) \approx S_{11}(t) + \Gamma_{LOAD} g(t - \tau_L) \quad (8)$$

where $g(t)$ is defined as the Inverse Fourier Transform of $S_{12}S_{21}$:

$$g(t) = \Im^{-1}\left(S_{12}(f)S_{21}(f)\right) = S_{12}(t) * S_{21}(t) \quad (9)$$

Since the structural mode $S_{11}(t)$ and $g(t)$ have finite time duration, the time responses associated to the structural mode and the tag mode $g(t-\tau_L)$ can be separated if the line length L is conveniently designed. The received signal at the reader in frequency domain is given by:

$$S_{tag}(f) = H_{free}(f, r_1)\Gamma_{in}(f)H_{free}(f, r_2)P(f) \quad (10)$$

where $P(f)$ is the Fourier Transform of the transmitted pulse $p(t)$ (which includes the response of the transmitting antenna), r_1 is the distance from the tag to the transmitting antenna, r_2 is the distance from the tag to the receiving antenna, and H_{free} is the transfer function due to free-space propagation:

$$H_{free}(f, r) = \frac{1}{\sqrt{4\pi} \cdot r} e^{-j2\pi f \cdot r/c} \xrightarrow{\Im^{-1}} h_{free}(t, r) = \frac{1}{\sqrt{4\pi} \cdot r} \delta(t - r/c) \quad (11)$$

where c is propagation velocity in free space, $r = r_1 + r_2$ and $\delta(t)$ is the Dirac delta function. The delay r/c represents the delay from the antenna, and the term $1/r$ represents the attenuation of a spherical wave. By applying the Inverse Fourier Transform to (10), the signal received at the reader in time domain is:

$$s_{tag}(t) = \Gamma_{in}(t) * h_{free}(t, r_1) * h_{free}(t, r_2) * p(t) \quad (12)$$

which can be expressed as:

$$\begin{aligned} s_{tag}(t) &= \alpha p(t - \tau_p) * S_{11}(t) + \alpha \cdot \Gamma_{LOAD} p(t - \tau_p) * g(t - \tau_L) \\ &= \alpha \cdot S_{11}(t) * p(t) * \delta(t - \tau_p) \\ &\quad + \alpha \cdot \Gamma_{LOAD} g(t) * p(t) * \delta(t - \tau_p - \tau_L) \end{aligned} \quad (13)$$

where α is the round-trip attenuation factor due to the propagation in free space and τ_p is the round-trip time delay between tag and reader. Both parameters are functions of the tag-reader distance r. In (13) $S_{11}(t) * p(t)$ is the response associated to the structural mode and $g(t) * p(t)$ is the response associated to the tag mode.

In the ideal case of an antenna with infinite bandwidth, $S_{11}(t)$ and $g(t)$ can be approximated by the Dirac delta function, $\delta(t)$. Then,

time resolution only depends on the type of pulse. However, the finite time duration of structural and tag modes produce an increase of the received pulse duration and some shape distortion, reducing the time resolution. This resolution determines the minimum delay that can be coded and, at the end, the number of data bits available.

In real measurements, tag response is distorted by clutter and cross-coupling between reader antennas. Clutter is defined as those scattering contributions not originated at the object under test (for instance, reflections at the walls or other objects). Then, the signal received at the reader can be expressed as:

$$s(t) = s_{tag}(t) + s_c(t) + s_m(t) \tag{14}$$

where $s_c(t)$ is coupling contribution and $s_m(t)$ is the clutter due to multipath reflections.

3. TIME-DOMAIN MEASUREMENT TECHNIQUES

Two measurement techniques are compared in this paper. They are mainly distinguished by the kind of stimulus signal that is applied.

3.1. Impulse Technique

In this technique, a UWB pulse is transmitted by the transmitting antenna. In order to concentrate the energy of the stimulus in the pass band of the antenna and therefore the UWB band, monocycles are used rather than pulses. The reflected signal at the tag $s(t)$ can be measured by means of an oscilloscope or a fast sampler. The experimental setup is shown in Figure 4.

Two UWB antennas, one for transmission and the other for reception, are pointed directly towards the tag. The GZ1120ME-50EV pulse generator (Geozondas) is used to generate a monocycle pulse with a central frequency of 5 GHz, an amplitude of ± 5 V and a pulse

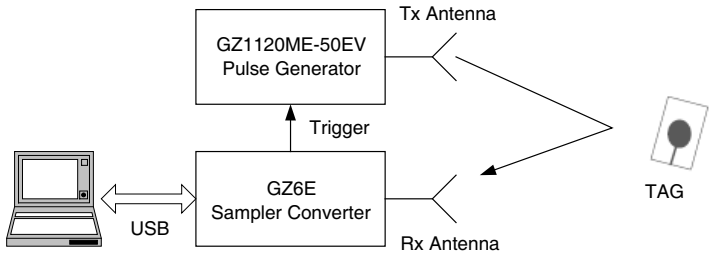

Figure 4. Experimental setup using a UWB radar.

repetition rate (PRI) of 250 KHz. Sampling is done with the GZ6E sampler converter (Geozondas), which triggers the pulse generator. More details about the waveforms are described in [33].

The mean energy of a UWB pulse is very low, even for relative high amplitudes, and the noise bandwidth of the sampling converters is very large. In consequence, this method is sensitive to random noise. Noise influence may be suppressed either by averaging (further reducing the measurement rate) or by generating extremely-high voltage impulses. However, this represents no practical solution for industrial applications. Another drawback arises in the inadequateness of the sampling gate control due to non-linearity in the ramp control, temperature drift or jitter. Possibly, UWB radars in the near future will overcome these drawbacks.

It is essential to reduce clutter in measurements to enhance the peak scattered at the tag using signal processing techniques and to reduce cross-coupling from the transmitter to the receiver. Two techniques have been used in the experiments to remove these unwanted contributions: background subtraction and time gating.

Assuming that clutter and cross coupling are stationary, their effect is reduced by subtracting the empty-room response (background) from the response in presence of the object. The second technique used to remove clutter from the measurement is gating, or time-domain windowing. All contributions that do not overlap with the object response are ignored. These contributions include reflections on the RF cables, walls, and interactions of the object with the room.

3.2. Step-frequency Technique

In this technique, a sine wave is frequency stepped or continuously swept over the band of interest. Figure 5 shows the experimental setup that has been implemented. The time-domain response is obtained from the Inverse Fourier Transform of the scattering parameter S_{21} measured with a vector network analyzer (in our setup Agilent PNA E8364C). The step width determines the unambiguous range. Attention should be paid to the Inverse Fourier Transform if the stimulus band is smaller than the antenna bandwidth. In this case, the side lobes in the impulse response are no longer determined by the antenna response but rather by the measurement bandwidth. These side lobes can be suppressed by windowing the data before the transformation, but doing these results in slightly reducing the range resolution (compared with using a rectangular window). In this work a Hamming window is used.

The advantages of the step-frequency technique are its excellent drift stability and random noise suppression because of the narrow-

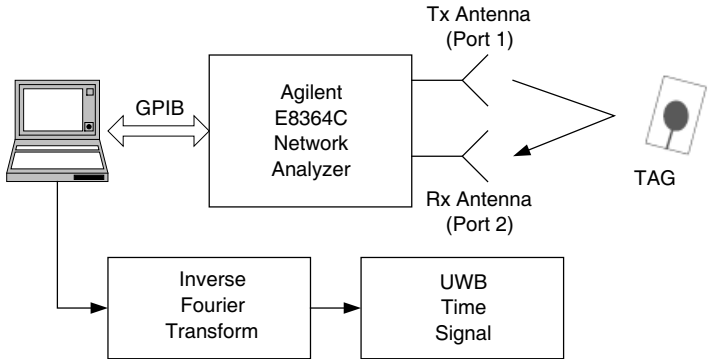

Figure 5. Experimental setup using a VNA.

band receivers, as well as its flexibility in the choice of the stimulus band. It is, however, the most expensive and slowest method. In order to reduce clutter, the same background subtraction and time-windowing techniques explained in Section 3.1 for the UWB radar are used.

4. EXPERIMENTAL RESULTS

In order to show the feasibility of time-domain measurements using the presented setups, a UWB time-coded chipless tag has been designed. The tag is composed by a circular slot UWB antenna [34–36] connected to one/several coaxial delay lines to easily adjust the delay. The proposed antenna is fabricated on Rogers4003 substrate, with relative dielectric permittivity $\varepsilon_r = 3.38$ and thickness $h = 32$ mil. Dimensions of the antenna and its photographs are shown in Figure 6. The radiation element consists of a circular slot of radius 35 mm that is fed by a circular open-ended microstrip line of radius 8.97 mm. This line is connected to the 50 Ω access line. Figure 7 shows measured and simulated $|S_{11}|$ and simulated maximum gain. Simulations are done with Agilent Momentum Electromagnetic Simulator. It can be observed that the antenna works correctly over the entire UWB band (3.1–10.6 GHz), with a $|S_{11}|$ under −10 dB.

Following the theory presented in Section 2, the structural backscattering mode is independent of the load connected to the antenna, whereas the antenna mode depends on the reflection coefficient of the load. Tag responses are measured at a distance of 50 cm when loading the antenna with different charges: a matched load (50 Ω), a short circuit and an open circuit. Measured time-

domain responses with the UWB radar setup and with the VNA setup can be observed in Figures 8(a)–(b) and 8(c)–(d), respectively. In Figures 8(a) and 8(c) both structural and tag modes can be observed. Tag modes are marked with a green circle in both figures, and zoomed in Figures 8(b) and 8(d). We can see that although the UWB radar is

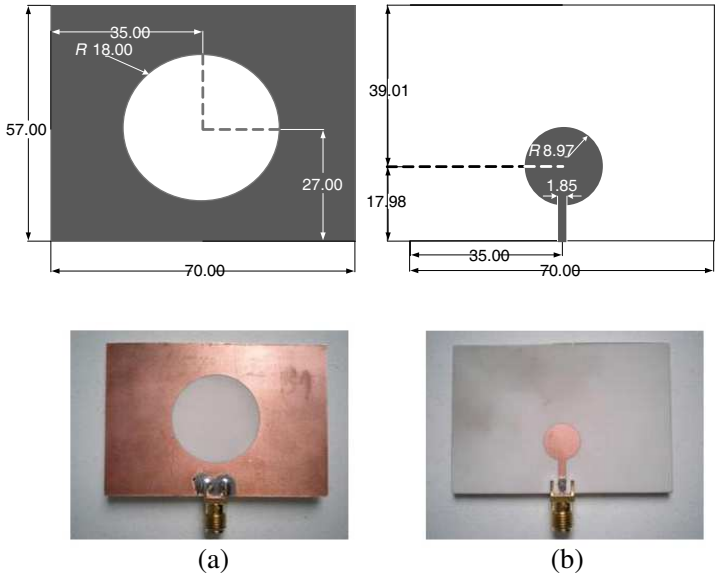

Figure 6. Layout and photographs of the designed antenna, (a) bottom face and (b) top face. Dimensions are in millimeters.

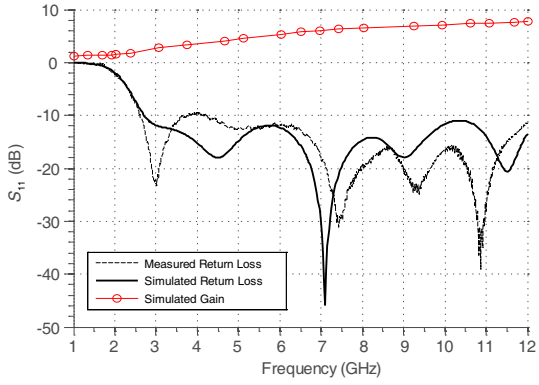

Figure 7. Simulated and measured $|S_{11}|$, and simulated maximum gain of the antenna.

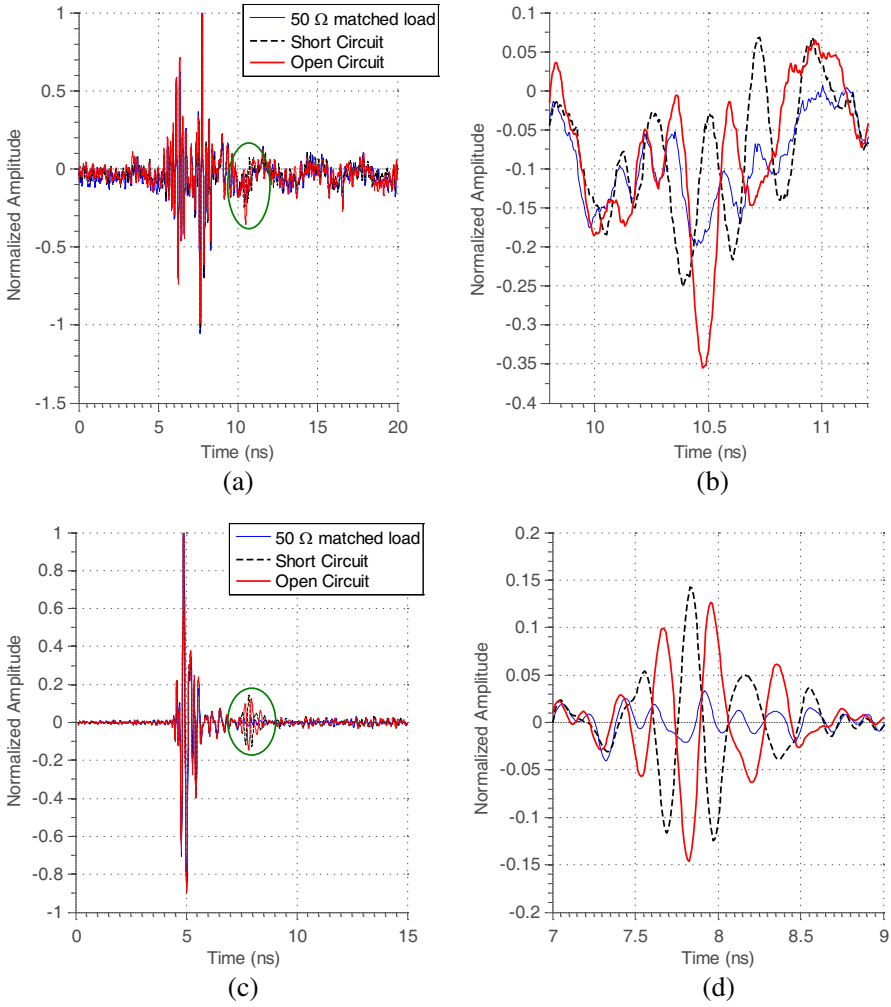

Figure 8. Tag response with different load conditions (matched, short-circuited and open-circuited load), (a)–(b) using a UWB Radar and (c)–(d) using a VNA.

noisier than the VNA, the expected results are perfectly visible. With a matched load, the pulse amplitude of the tag mode is minimum, while with a short or open circuit load the amplitude is maximum but with opposite sign. This is explained since $\Gamma_{LOAD} = 1$ for an open circuit and $\Gamma_{LOAD} = -1$ for a short circuit. The results obtained with the VNA and the UWB radar agree with similar results obtained only with a VNA in [12, 14–17], and they show that the tag mode can

be modulated in amplitude. It is also clear that if the delay of the transmission line is large enough, the structural and antenna modes can be split.

However, one of the objectives of this work is to go beyond from detecting modulations in amplitude since in time-domain chipless RFID the information must be coded in the time difference between structural and tag modes. To analyze the time-domain response with different delays, the tag is loaded with open-ended transmission lines with different lengths, which implies different delays between the structural and tag modes. Seven delays are measured, increasing the transmission line length on each delay. Each measurement or delay is labeled from 1 to 7. In these experiments, the distance between the tag and the reader is 1.5 meters. All the experiments have been performed in our laboratory without using any anechoic chamber in order to simulate practical operation in a real RFID application.

Figures 9(a) and 9(b) show the measurements for the UWB radar setup and for the VNA setup, respectively. Again, the VNA gives a cleaner signal, but in both graphs it can be observed that the peaks of the tag mode (marked with a red circle) are detected at different delays for each delay number, while the structural mode peak remains always at the same delay (at about 6.3 nanoseconds for the UWB radar and at 10.3 nanoseconds for the VNA). The change in the tag mode delay is clearly visible between delays 4 and 5, where the transmission line length increase is higher.

Finally, Table 1 and Figure 10 show a comparison between the

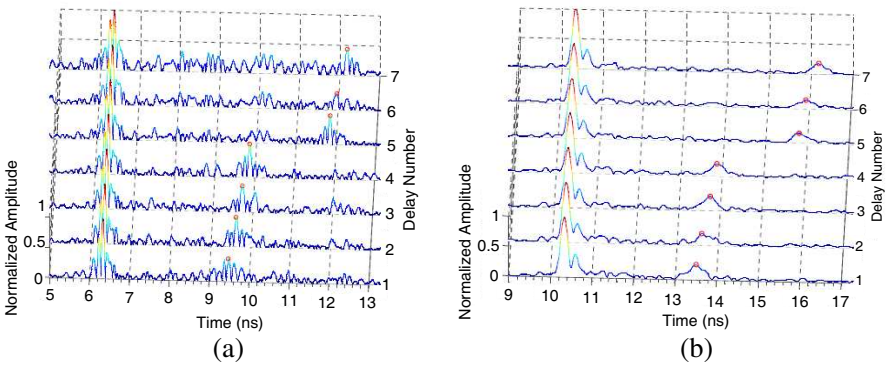

Figure 9. Structural mode and tag mode for the tag with different transmission line lengths, for (a) the UWB radar and (b) the VNA. The tag-to-reader distance is 1.5 m. Each tag mode peak is marked with a circle.

Table 1. Comparison between the detected delays for both topologies (UWB radar and VNA) and theoretical delays (tag-to-reader distance of 1.5 m) and Standard Deviation for each delay number, considering theoretical and measured delays.

Delay Number	Length (mm)	Delay value (ns)			Standard Deviation (ps)
		IR-UWB Radar	VNA	Theoretical Value	
1	252.0	2.685	2.685	2.685	0
2	279.3	2.837	2.779	2.763	38.9
3	306.6	2.944	2.934	2.996	33.3
4	333.9	3.076	3.043	3.156	58.1
5	513.1	5.054	4.972	5.132	80.0
6	540.4	5.181	5.096	5.214	60.9
7	567.7	5.386	5.360	5.374	13.0

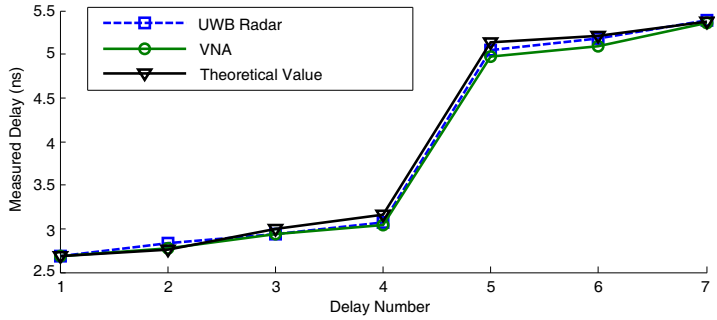

Figure 10. Comparison between the detected delays for both topologies (UWB radar and VNA) and theoretical delays (tag-to-reader distance of 1.5 m).

detected differential delays between tag and structural modes for each measurement (Delay Number). The theoretical delay is the real physical delay of the transmission line. Since the first delay (2.685 ns) is due to the reflection of the tag without any transmission line connected to it, the delay is always the same for all setups, and it is used as a reference for the following ones. It is shown that even though the measured delays with the two setups are not exactly the same as the theoretical ones, their values are very similar and their growing trend, (i.e., no delay is lower than its predecessor) is the same. Last column of Table 1 shows the Standard Deviation, in picoseconds, of

the experimental results. It can be seen a maximum deviation of about 80 ps that appears at the fifth delay.

The previous results show that delay changes of about 150 ps (which are comparable to pulse duration) can be detected in both systems. It can be seen also that there is a relatively high Standard Deviation for some delays (for example, 80 ps for delay 5, as commented), which could lead to measurement errors compared to the resolution of 150 ps. However, all measured delays for each measurement setup are slightly higher than the theoretical values, so no delay can overlap its adjacent one. Hence as expected from theory presented in Section 2, the delay resolution is limited by the received pulse waveform. Thus, the number of bits depends of this parameter and the maximum delay allowed (which depends on the transmission losses, the receiver noise and residual clutter interference not compensated in the calibration). For instance, in the particular example shown in this work up to 18 states can be coded (considering a resolution of 150 ps and delays between 2.6 and 5.4 ns). However, the number of states depends not only on the resolution, but on the time window used. A time window of up to 25 ns was used in the measurements, which sets the theoretical upper limit to 166 coded states. The time window could be higher than 25 ns, but it is limited by free-space propagation and the pulse repetition interval (PRI). Since a pulse repetition frequency (PRF) of 250 kHz is used, the PRI is 4000 ns, so the real limitation is free-space propagation. Finally, more states could be coded if the variations were made not only in terms of time, but also in terms of amplitude, which is possible according to the results given in Figure 8. Nevertheless, these tags potential resides into using them for integrated remote sensors or semi-passive RFID, not into the number of states that can be coded.

5. CONCLUSIONS

This work has theoretically and empirically shown the feasibility for time-domain UWB RFID detection. Experimental results confirm that not only amplitude changes are detectable, (i.e., with a short circuit, open circuit, or matched load), but also different delays by means of different lengths for transmission lines. This permits the detection of the delay between structural and tag modes, therefore making tag codification possible. Two experimental setups for time-domain detection have been compared. Although the VNA-based setup presents less noise, this topology is prohibitive for low-cost UWB readers. In consequence the new presented setup, based on a IR-UWB radar is more interesting from a commercial point of view, since low-

cost integrated circuits for UWB receivers are coming nowadays and in the near future. In addition, it has been demonstrated that read-ranges of about 1.5 m are possible using the two methods (VNA and UWB radar). These read-ranges are larger compared with the read-ranges of the order of tens of centimeters demonstrated for frequency-coded chipless tags measured with a VNA in [10, 11]. This order of magnitude for the read-ranges and future low-cost readers based on UWB radars open the door to practical applications for this technology.

REFERENCES

1. Finkenzeller, K., *RFID Handbook: Fundamentals and Applications in Contactless Smart Cards, Radio Frequency Identification and Near-field Communication*, 3rd Edition, Wiley, 2010.
2. Vita, G. D. and G. Iannaccone, "Design criteria for the RF section of UHF and microwave passive RFID transponders," *IEEE Trans. on Microwave Theory and Tech.*, Vol. 53, No. 9, 2978–2990, 2005.
3. Collins, J., "Alien cuts tag price," *RFID J.*, Apr. 2004. [Online]. Available: http://www.rfidjournal.com/article/articleview/857/1/1/, (accessed Apr. 2008).
4. Lazaro, A., D. Girbau, and R. Villarino, "Effects of interferences in UHF RFID systems," *Progress In Electromagnetic Research*, Vol. 98, 435–443, 2009.
5. Lazaro, A., D. Girbau, and D. Salinas, "Radio link budgets for UHF RFID on multipath environments," *IEEE Trans. on Antennas and Prop.*, Vol. 57, No. 4, 1241–1251, 2009.
6. Lorenzo, J., D. Girbau, A. Lazaro, and R. Villarino, "Read range reduction in UHF RFID due to antenna detuning and gain penalty," *Microwave and Optical Technology Letters*, Vol. 53, No. 1, 144–148, 2011.
7. Lazaro, A., D. Girbau, and R. Villarino, "Wavelet-based breast tumor localization technique using a UWB radar," *Progress In Electromagnetics Research*, Vol. 98, 75–95, 2009.
8. Fontana, R. J., "Recent system applications of short-pulse ultra-wideband (UWB) technology," *IEEE Trans. on Microwave Theory and Tech.*, Vol. 52, No. 9, 2087–2104, Sep. 2004.
9. Sahinoglu, Z., S. Gezici, and I. Guvenc, *Ultra-wideband Positioning Systems*, Cambridge University Press, 2008.
10. Preradovic, S., I. Balbin, N. C. Karmakar, and G. F. Swiegers, "Multiresonator-based chipless RFID system for low-cost item tracking," *IEEE Trans. on Microwave Theory and Tech.*, Vol. 57, No. 5, 1411–1419, May 2009.

11. Balbin, I. and N. Karmakar, "Novel chipless RFID tag for conveyor belt tracking using multi-resonant dipole antenna," *Proceedings of the 39th European Microwave Conference*, 1109–1112, Oct. 2009.
12. Hu, S., Y. Zhou, C. L. Law, and W. Dou, "Study of a uniplanar monopole antenna for passive chipless UWB-RFID localization system," *IEEE Trans. Antennas Propag.*, Vol. 58, No. 2, 271–278, 2010.
13. Zhang, L., S. Rodriguez, H. Tenhunen, and L.-R. Zheng, "An innovative fully printable RFID technology based on high speed time-domain reflection," *HDP'06, Conference on High Density Microsystem Design and Packaging and Component Failure Analysis*, 166–170, 2006.
14. Hu, S., C. L. Law, and W. Dou, "Petaloid antenna for passive UWB-RFID tags," *Electronics Letters*, Vol. 43, No. 22, Oct. 2007.
15. Hu, S., C. L. Law, and W. Dou, "A balloon-shaped monopole antenna for passive UWB-RFID tag applications," *IEEE Antennas and Wireless Propagation Letters*, Vol. 7, 366–368, 2008.
16. Hu, S., Y. Zou, C. L. Law, and W. Dou, *IEEE Trans. Antennas Propag.*, Vol. 58, No. 2, 271–278, 2010.
17. Dardari, D. and R. D'Errico, "Passive ultrawide bandwidth RFID," *IEEE Global Telecommunications Conference (GLOBECOM)*, 1–6, 2008.
18. Hartmann, C. S., "A global SAW ID tag with large data capacity," *Proc. IEEE Ultrason. Symp.*, Vol. 1, 65–69, Munich, Germany, Oct. 2002.
19. Reindl, L., G. Scholl, T. Ostertag, H. Scherr, U. Wolff, and F. Schmidt, "Theory and application of passive SAW radio transponders as sensors," *IEEE Trans. on Ultrasonics, Ferroelectrics, and Frequency Control*, Vol. 45, No. 5, 1281–1292, Sep. 1998.
20. Reindl, L., C. C. W. Ruppel, S. Berek, U. Knauer, M. Vossiek, P. Heide, and L. Oréans, "Design, fabrication, and application of precise SAW delay lines used in an FMCW radar system," *IEEE Trans. on Microwave Theory and Tech.*, Vol. 49, No. 4, 787–794, Apr. 2001.
21. Rao, K. V. S., P. V. Nikitin, and S. M. Lam, "Antenna design for UHF RFID tags: A review and a practical application," *IEEE Trans. on Antennas and Prop.*, Vol. 53, No. 12, 3870–3876, Dec. 2005.
22. Green, R. B., "Relationships between antennas as scatterers and

radiators," *IEEE Trans. on Antennas and Prop.*, Vol. 14, No. 1, 17–21, Jan. 1966.

23. Collin, R. E. and F. Zucker, *The Receiving Antenna, Antenna Theory*, Part 1, McGraw-Hill, New-York, 1969.
24. Hansen, R. C., "Scattering from conjugate-matched antennas," *Proceedings of the IEEE*, Vol. 77, No. 5, 659–662, May 1989.
25. Hong, T., S.CX. Gong, W. Jiang, Y.-X. Xu, and X. Wang, "A novel ultra-wide band antenna with reduced radar cross section," *Progress In Electromagnetics Research*, Vol. 96, 299–308, 2009.
26. Marynowski, W. and J. Mazur, "Design of uwb coplanar antenna with reduced ground plane," *Journal of Electromagnetic Waves and Applications*, Vol. 23, No. 13, 1707–1713, 2009.
27. Jiang, W., S.-X. Gong, Y.-P. Li, T. Hong, X. Wang, and L.-T. Jiang, "A novel low RCS mobius-band monopole antenna," *Journal of Electromagnetic Waves and Applications*, Vol. 23, No. 14/15, 1887–1895, 2009.
28. Jiang, W., T. Hong, Y. Liu, S.-X. Gong, Y. Guan, and S. Cui, "A novel technique for radar cross section reduction of printed antennas," *Journal of Electromagnetic Waves and Applications*, Vol. 24, No. 1, 51–60, 2010.
29. Liu, Y., D. M. Fu, and S. X. Gong, "A novel model for analyzing the radar cross section of microstrip antenna," *Journal of Electromagnetic Waves and Applications*, Vol. 17, No. 9, 1301–1310, 2003.
30. Johnson, J. H., W. Choi, and R. L. Moore, "Precision experimental characterization of the scattering and radiation properties of antennas," *IEEE Trans. on Antennas and Prop.*, Vol. 30, 108–112, 1982.
31. Liang, J. X., C. C. Chian, X. D. Chen, and C. G. Parini, "Study of a printed circular disc monopole antenna for UWB systems," *IEEE Trans. on Antennas and Prop.*, Vol. 53, No. 11, 3500–3504, Nov. 2005.
32. Yang, C., Q. Guo, and K. Huang, "Study of a double-feed circular disc monipole antenna for UWB systems," *Journal of Electromagnetic Waves and Applications*, Vol. 24, No. 14/15, 1943–1952, 2010.
33. Lazaro, A., D. Girbau, and R. Villarino, "Analysis of vital signs monitoring using an IR-UWB radar," *Progress In Electromagnetics Research*, Vol. 100, 265–284, 2010.
34. Angelopoulos, S., A. Z. Anastopoulos, D. I. Kaklamani, A. A. Alexandridis, F. Lazarakis, and K. Dangakis, "Circular

and elliptical CPW-fed slot and microstrip-fed antennas for ultra wideband applications," *IEEE Antennas and Wireless Propagation Letters*, Vol. 5, 294–297, 2006.

35. Barbarino, S. and F. Consoli, "Uwb circular slot antenna provided with an inverted-l notch filter for the 5 GHz WLAN band," *Progress In Electromagnetics Research*, Vol. 104, 1–13, 2010.
36. Chen, D. and C. H. Cheng, "A novel compact ultra-wideband (UWB) wide slot antenna with via holes," *Progress In Electromagnetics Research*, Vol. 94, 343–349, 2009.